Delft University of Technology
Department of Aerospace Engineering

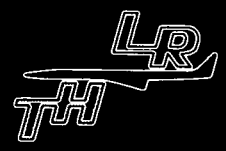

Report LR-416

NUMERICAL SOLUTION OF TRANSONIC NORMAL SHOCK WAVE-BOUNDARY LAYER INTERACTION USING THE BOHNING-ZIEREP MODEL

B. Koren and W.J. Bannink

Delft - The Netherlands

January 1984

Delft University of Technology
Department of Aerospace Engineering

Report LR-416

NUMERICAL SOLUTION OF TRANSONIC NORMAL SHOCK WAVE-BOUNDARY LAYER INTERACTION USING THE BOHNING-ZIEREP MODEL

B. Koren and W.J. Bannink

Delft - The Netherlands

January

SUMMARY

The present report describes a numerical method for transonic shock wave-boundary layer interaction on a plane wall or on a convex wall. The method is based on the Bohning-Zierep model (Ref. 1), where a turbulent boundary layer is perturbed by a weak normal shock wave that exists in the external flow. The flow region along the wall is divided into a relatively thick upper layer, where the flow is considered to be inviscid and rotational, and a thin sublayer where the flow is viscous. The problem of the diffusion inside these layers of the jumps in flow quantities across the shock wave has been solved analytically by Bohning and Zierep assuming a basic flow that is perturbed by the presence of a weak shock wave. In the numerical procedure the practical disadvantages of the analytical method are avoided. These disadvantages are: its restriction to a limited form of input data (a power law velocity profile) that allows the problem to be handled analytically using the very specific hypergeometric functions.

The present results appear completely within the band of the analytical and of other numerical solutions. Compared to experimental data on a plane wall as well as on a convex wall, a good agreement is obtained as long as the Mach number in front of the shock wave does not exceed unity too much, which may be expected since it is inherent to the perturbation model.

CONTENTS

LIST OF SYMBOLS

a	speed of sound
c_f	skinfriction coefficient
$f_i(x,y)$ $f_j(x,y)$	linear elementary function, used in the finite element method
K	von Kármán constant
ℓ	half length of region of interaction
L	half length of region of integration
M	Mach number
M_o	Mach number of basic flow
M_o^*	velocity of basic flow, non-dimensionalized by critical speed of sound
p	pressure
p_o	pressure of basic flow, non-dimensionalized by critical pressure
p'	perturbation pressure, non-dimensionalized by critical pressure
p_{t_1}	total pressure ahead of shock wave
Pr	Prandtl number
r	coordinate; recovery factor
R_w	radius of curvature of the wall
Re_δ	Reynolds number based on boundary layer thickness and at critical flow conditions
s_{10}	free parameter, eq. (17)
T_o	temperature of basic flow, non-dimensionalized by critical temperature
T'	perturbation temperature, non-dimensionalized by critical temperature
u	velocity component in x-direction
u'	perturbation velocity component in x-direction, non-dimensionalized by critical speed of sound
v	velocity component in y-direction
v'	perturbation velocity component in y-direction, non-dimensionalized by critical speed of sound
$w_j(x,y)$	weight function, eq. (23)
x,y	cartesian coordinates, Fig. 2, non-dimensionalized by ℓ and δ, respectively
x_o	x-coordinate of shock wave front
x_1	$\frac{1 - x_o}{5}$
x_i, y_i	position of meshpoints

x_{i3}	third meshpoint after x_1
y_o	thickness of sublayer, non-dimensionalized by boundary layer thickness
α	exponent in power law velocity profile of Bohning and Zierep (Ref. 1)
γ	ratio of specific heats
δ	thickness of incoming boundary layer of basic flow
δ_μ	thickness of viscous sublayer
ρ_o	density of basic flow, non-dimensionalized by critical density
ρ'	perturbation density, non-dimensionalized by critical density
τ_w	wall shear stress
φ	function defined in eq. (6); polar angle
φ_i	φ in nodes of triangular elements
φ_N	approximation of φ

Subscripts

o	basic flow quantities

Superscripts

*	critical flow conditions
^	flow quantities immediately downstream of shock wave
'	perturbation quantities

1. INTRODUCTION

The problem of transonic shock wave-boundary layer interaction on a curved wall has been treated analytically by Bohning and Zierep (Ref. 1). They based their flow model on the experimental investigations made in 1946 by Ackeret, Feldmann and Rott (Ref. 2) who investigated the interaction of a normal shock with the boundary layer on a curved wall. The experiments indicated a singular behaviour of the pressure gradient immediately downstream of the shock, manifesting itself in an expansion at the outer edge of the turbulent boundary layer. This rather pronounced expansion at the boundary layer edge decreased more and more in a diffusion process when approaching the wall, and also induced an upstream effect in the boundary layer.

The after-expansion is also observed in the inviscid case at the downstream foot of a normal shock wave on a curved surface. Oswatitsch and Zierep (Ref. 3) solved this problem locally by means of a series expansion of the perturbation potential in transonic flow.
They found that at a convex surface the normal shock wave curves upstream (downstream at a concave surface), whereas at the foot the curvature is logarithmically infinite. As a consequence the velocity and the pressure gradient show a logarithmic singularity resulting in an expansion immediately downstream of the shock wave.

Inspired by the similarity between the experimental results of Ackeret, Feldmann and Rott (Ref. 2) and the inviscid solution of Oswatitsch and Zierep (Ref. 3) Bohning and Zierep (Ref. 1) developed an analytical method to introduce the Oswatitsch-Zierep singularity into a viscous model. However, it should be mentioned that the influence of viscosity in the Bohning-Zierep model is restricted to a very thin sublayer, with a thickness of the order of one hundredth of the actual boundary layer thickness.

The numerical method described in this report is entirely based on the Bohning-Zierep flow model. The advantage of the computational approach may be found in the fact that a more general flow field can be covered. Where Bohning and Zierep only could select a special initial velocity profile of the boundary layer (a profile that nevertheless is rather realistic) and yet gives rise to a rather complicated analysis, a computational approach might generalize the problem without more complexity.

Without going into the extensive description of the Bohning-Zierep model the numerical method will be described in the following.

Where in the course of the numerical treatment a completion or readjustment of the model and its equations is necessary or possible it is indicated.

2. THE BOHNING-ZIEREP FLOW MODEL

2.1. General description

In their description of the normal shock wave-boundary layer interaction at a convex surface Bohning and Zierep (Ref. 1) consider a region (Fig. 1) extending at a distance ℓ upstream and downstream of the shock wave. ℓ is of the order of the boundary layer thickness. At the upstream end of the region a boundary layer of the basic flow ("Grundströmung", as they call it) enters the region with a prescribed velocity profile. The thickness of the layer to the level where the velocity is sonic is called δ. The basic flow is considered independent of the distance along the wall (wall curvature << 1). At the upper edge δ of the region a weak transonic shock wave ends.

The region is divided into two layers:

- a thick inviscid upper layer (the only "viscous" effect is contained in the entering velocity profile).
- a thin sublayer with thickness δ_μ.

The thickness δ_μ depends upon the entering velocity profile and upon the Reynolds number based on δ. δ_μ is unknown and has to be determined in the analysis.

The flow is composed of the above mentioned basic flow and a perturbation flow. The basic flow, which is known, remains when the shock wave strength vanishes and, therefore, the perturbation flow, which has to be determined, exists only because of the presence of the shock wave. The perturbation quantities are considered small with respect to the basic flow quantities.

2.2. Perturbation equations in the inviscid upper layer

According to Ref. 1 a cartesian coordinate system is introduced shown in Fig. 2, and the perturbation equations for the inviscid upper layer may be written as follows,
the continuity equation:

$$\rho_o \frac{\partial u'}{\partial x} + M_o^* \frac{\partial \rho'}{\partial x} + \frac{\ell}{\delta} \frac{\partial (\rho_o v')}{\partial y} = 0 \quad ^{1)} \tag{1}$$

the momentum equations:

$$\rho_o M_o^* \frac{\partial u'}{\partial x} + \rho_o v' \frac{\ell}{\delta} \frac{dM_o^*}{dy} + \frac{1}{\gamma} \frac{\partial p'}{\partial x} = 0 \tag{2}$$

$$\rho_o M_o^* \frac{\partial v'}{\partial x} + \frac{1}{\gamma} \frac{\ell}{\delta} \frac{\partial p'}{\partial y} = 0 \tag{3}$$

---

1) In this report the ratio ℓ/δ is maintained throughout the computations

the energy equation:

$$T' + (\gamma - 1)\, M_o^*\, u' = 0 \tag{4}$$

the equation of state:

$$\rho_o T' + \rho' T_o = p' \tag{5}$$

In these equations all flow quantities are non-dimensionalized by their critical values; the subscript o and the prime denote basic flow and perturbation flow quantities respectively. Thus, the non-dimensional velocity components are given by $M_o^* + u'$ and v'; the non-dimensional pressure, density and temperature by $p_o + p'$, $\rho_o + \rho'$, $T_o + T'$ respectively. The x-coordinate is non-dimensionalized by ℓ, a characteristic length in x-direction, and the y-coordinate is non-dimensionalized by δ, the already mentioned y level where the flow velocity is sonic.

2.3. The boundary value problem for the inviscid upper layer

By putting

$$p' = -\gamma \frac{\partial \varphi}{\partial x}\,, \quad v' = \frac{\ell}{\delta} \frac{1}{\rho_o M_o^*} \frac{\partial \varphi}{\partial y} \tag{6}$$

according to Ref. 1, we obtain for eqs. (1), (2), (3) the single equation

$$\left(\frac{\ell}{\delta}\right)^2 \varphi_{yy} - (M_o^2 - 1)\, \varphi_{xx} - \left(\frac{\ell}{\delta}\right)^2 \frac{2}{M_o} \frac{dM_o}{dy}\, \varphi_y = 0 \tag{7}$$

The region where eq. (7) is integrated is shown in Fig. 3 and the boundary conditions are:

1. at $x = \pm L$ the y component of the velocity vanishes, giving

$$\varphi_y\,(-L,y) = \varphi_y(L,y) = 0 \tag{8}$$

2. at the outer edge, $y = 1$, of the upper inviscid layer the perturbation pressure p' is prescribed by the external flow, thus

$$\varphi_x(x,1) = -\frac{1}{\gamma}\, p'(x,1) \tag{9}$$

3. at the inner edge, $y = y_o$, we have $\dfrac{\partial p'(x,y_o)}{\partial y} = 0$, so that, with eqs. (3) and (8)

$$\varphi_y(x,y_o) = 0 \tag{10}$$

Eqs. (8) and (9) may be integrated at $x = \pm L$ and at $y = 1$, resulting in

$$\varphi(-L,y) = C \tag{11}$$

$$\varphi(x,1) = C - \frac{1}{\gamma}\int_{-L}^{x} p'(\xi,1)\, d\xi \tag{12}$$

$$\varphi(L,y) = C - \frac{1}{\gamma}\int_{-L}^{L} p'(\xi,1)\, d\xi \tag{13}$$

where C is an undetermined constant. Since, in the analysis only derivatives of φ are concerned, C will not be determined.

The thickness y_o of the viscous sublayer, occurring in the boundary condition given by eq. (10) is determined completely according to Ref. 1, where y_o is given as

$$y_o = \frac{\delta_\mu}{\delta} \tag{14}$$

In Ref. 1 the x derivative of the wall shear stress τ_w is taken as the characteristic physical quantity of which the parametric dependance of y_o is analysed; this derivative is expressed as

$$\frac{1}{a^*}\frac{\partial \tau_w}{\partial x} = \mu \frac{\partial^2 u'(y_o,x,0)}{\partial x \partial y} \tag{15}$$

y_o may be considered as the y position where the viscous and inviscid forces balance; above y_o the inertia forces are dominant, below that value this is the case with the viscous forces.
Following Ref. 1 and taking into account the ratio $\frac{\ell}{\delta}$ we find

$$u'(x,y) = \frac{\delta}{\ell}\, Re_\delta \frac{dp'(x,y_o)}{dx}\frac{y_o^2}{2}\left\{-\frac{M_o^2(y_o)}{6}\left(\frac{y}{y_o}\right)^4 + \frac{1}{\gamma}\left(\frac{y}{y_o}\right)^2 + \right.$$

$$\left. + \frac{M_o^2(y_o)}{6}\frac{y}{y_o} - \frac{1}{\gamma}\frac{y}{y_o}\right\} + u'(x,y_o)\frac{y}{y_o} \tag{16}$$

Now, y_o is determined from eqs. (15) and (16) by taking

$$\frac{\partial}{\partial y_o}\left\{\frac{\partial^2 u'(0,0)}{\partial x \partial y}\right\} = 0 \tag{15'}$$

In the numerical compution, which will be discissed later, eq. (15) appeared to have such an extremum.
y_o is of the order of 1% of the boundary layer thickness.

For the pressure prescribed at the outer edge of the upper inviscid layer downstream of the incident shock the expressions of the Oswatitsch-Zierep theory (Refs. 1,3) are used. Translated into our system for $r = x$, $\varphi = 0$ (Fig. 4) these equations read

$$\hat{u}'(x,1) = \hat{u}'(0,1) - \frac{1}{\pi \sqrt{1 - \hat{M}^2(0,1)}} \left\{ \frac{2\ell}{R_w} - \frac{\partial \hat{v}'(0,1)}{\partial x} \right\} (2x \ln x + x) - 4 s_{10} \hat{u}'(0,1)\, x \tag{17}$$

$$\hat{v}'(x,1) = - \left\{ \frac{\ell}{R_w} - \frac{\partial \hat{v}'(0,1)}{\partial x} \right\} x \tag{18}$$

where $\hat{}$ denotes quantities downstream of the shock wave, R_w is the radius of curvature of the wall and s_{10} is a free parameter matching the boundary layer flow to the external flowfield.

Integrating the momentum equation (2) with respect to x we obtain

$$\hat{p}'(x,1) = -\gamma \rho_o(1)\, M_o^*(1) \{\hat{u}'(x,1) - \hat{u}'(0,1)\} + - \gamma \rho_o(1) \frac{\ell}{\delta} \frac{dM_o^*(1)}{dy} \int_0^x \hat{v}'(\xi,1)\, d\xi + \hat{p}'(0,1) \tag{19}$$

Since $\hat{p}'(x,1)$ is not known a priori, it requires a known flow in the inviscid upper layer (and vice versa, the determination of the flow field in the inviscid upper layer requires known values of $\hat{p}'$ at the edge of the layer); it has to be determined iteratively.

3. COMPUTATIONAL METHOD

3.1. Boundary value problem

The boundary value problem given by eqs. (7) and (10)-(13) together with eq. (19) has been solved numerically for C = 0 and, according to Ref. 1, for δ/ℓ has been taken the value 0.44.

The numerical treatment allows a more realistic incoming velocity profile at x = -L than the power law

$$M_o(y) = y^{\alpha}$$

of Ref. 1. In the present case we adopted the turbulent boundary layer profile

$$M_o^*(y) = M_o^*(1) \left[1 + \frac{1}{K}\sqrt{\frac{c_f(-L)}{2}\left\{1 + r\,\frac{\gamma - 1}{2}\,M^2(-L,1)\right\}} \cdot \right.$$
$$\left. \cdot \left\{\ln y - 0{,}5(1 + \cos \pi y)\right\}\right] \qquad (20)$$

In eq. (20)

$$M_o^* = \sqrt{\frac{(\gamma + 1)\,M_o^2}{2 + (\gamma - 1)\,M_o^2}}\,;$$

$M_o^*(1) = 1$, according to Ref. 1; K = 0.41, the von Kármán constant; $c_f(-L)$ is the skin friction coefficient at x = -L; r = 0.89, the recovery coefficient for a turbulent boundary layer; M(-L,1) is the Mach number of the complete flow (basic flow plus perturbation) at the edge of the boundary layer at x = -L. The term ln y describes the logarithmic law of the wall of the incoming velocity profile; (1 + cos πy) is the additional term of the Coles wake function, it is multiplied by 0.5 in the case of a turbulent boundary layer without pressure gradient.

3.2. Method of solution

For the solution of the problem a finite element approach has been used, developed at the Department of Mathematics, University of Technology Delft. The method consists of a package of Fortran subroutines applicable to boundary value problems to be solved with finite element methods. This package called AFEP (A Finite Element Package) is described in detail in Refs. 4, 5 and 6; only its application on the present problem will be described shortly in this report.

The computational domain is subdivided in a number of subdomains,

shown in Fig. 5, each with its own meshpoint distribution. The number of meshpoints n_i on a subboundary i is indicated in Fig. 5 as i, n_i; the total number of meshpoints is 1121.

The shock wave at the outer edge of the inviscid upper layer is confined within the interval $-x_o, x_o$ ($x_o = 10^{-6}$), then the numerical pressure rise is almost discontinuous.

In regions where the derivatives of flow quantities are large a fine meshwidth has been chosen, thus

$$x_1 = \frac{1 - x_o}{5} \quad \text{and} \quad y_1 = \frac{1 - y_o}{10}$$

The streamwise dimension of the computational domain is taken as $L = 10$.

The computational domain now is divided into triangular elements, the corner points of which are the above mentioned meshpoints. In each point the value of φ, φ_i, is considered; φ_i is known at the boundaries.

In the numerical procedure an approaching solution of φ is introduced by

$$\varphi_N(x,y) = \sum_{i=1}^{N} \varphi_i f_i(x,y) \tag{21}$$

where $N = 1121$ is the total number of meshpoints, and $f_i(x,y)$ are elementary functions, which are linear since each element covers three meshpoints (Fig. 6). The functions $f_i(x,y)$ are given by

$$f_i(x_i, y_i) = 1$$

$$f_i(x,y) = 0 \quad \text{for all other meshpoints given in Fig. 6}$$

If eq. (21) is substituted into eq. (7) we obtain

$$\left(\frac{\ell}{\delta}\right)^2 (\varphi_N)_{yy} - (M_o^2 - 1)\,(\varphi_N)_{xx} - \left(\frac{\ell}{\delta}\right)^2 \frac{2}{M_o}\,(\varphi_N)_y = R(\varphi_N) \tag{22}$$

The residual $R(\varphi_N)$ should be made as small as possible. This is achieved by selecting N independent weight functions $w_j(x,y)$ and to require that

$$\int_{y_o}^{1} \int_{-L}^{L} w_j(x,y)\, R\{\varphi_N(x,y)\}\, dxdy = 0\,, \quad j = 1, 2, 3 \ldots N \tag{23}$$

In most applications, for the weight functions the elementary functions

are taken; then, combining eqs. (21), (22) and (23) we obtain the system of Galerkin equations

$$\sum_{i=1}^{N} \varphi_i \int_{y_o}^{1} \int_{-L}^{L} f_j \left\{ \left(\frac{\ell}{\delta}\right)^2 \frac{\partial^2 f_i}{\partial y^2} - (M_o^2 - 1) \frac{\partial^2 f_i}{\partial x^2} + \right.$$

$$\left. - \left(\frac{\ell}{\delta}\right)^2 \frac{2}{M_o} \frac{dM_o}{dy} \frac{\partial f_i}{\partial y} \right\} dxdy = 0 \qquad (24)$$

where $j = 1, 2, 3 \ldots N$.

Integration by parts in two dimensions of eq. (24) and using the boundary conditions, eqs. (10)-(13), enables us to rewrite the homogeneous system of (linear algebraic) Galerkin equations into an inhomogeneous system. The right hand sides of these equations appear by evaluation of the integrated terms in the expressions of the integration by parts. (The AFEP subroutine procedure is such that the process with the elementary functions and the integration by parts is incorporated in the procedure.)

The solution of the inhomogeneous system of linear algebraic equations provides the values φ_i, from which φ_N may be obtained. The problem, involving an asymmetric band matrix, is solved by means of a profile - LDU - decomposition method.

3.3. Application of the boundary conditions along the upper and lower boundaries of the inviscid layer

3.3.1. The thickness of the viscous sublayer

In the numerical computation of the flow in the inviscid upper layer the determination of the thickness y_o of the viscous sublayer is part of the solution procedure. According to Ref. 1 (see paragraph 2.3. of the present report) the determination of y_o is part of the solution process for the flow in the inviscid upper layer. Since $y_o = O(0.01)$ (Ref. 1), as an initial guess y_o is assumed to belong to the interval $0.005 \leq y_o \leq 0.015$. Then, for three distinct values of y_o, displayed regularly in that interval, the boundary value problem for φ is solved, yielding the u' and p' distributions along the edge of the sublayer. Using the mixed derivative of eq. (16) we may now compute

$$\frac{\partial^2 u'(0,0)}{\partial x \partial y}$$

necessary for the determination of $(y_o)_{min}$, for each of the distinct values of y_o. Writing

$$\frac{\partial^2 u'(0,0)}{\partial x \partial y}$$

as a quadratic function

$$\frac{\partial^2 u'(0,0)}{\partial x \partial y} = a y_o^2 + b y_o + c \qquad (25)$$

when a, b, c are constants to be determined.

Then, the minimum value for y_o is found to be

$$(y_o)_{min} = - \frac{b}{2a}$$

Of course $(y_o)_{min}$ should ly within the afore mentioned interval, if this is not so the procedure should be repeated for a new interval of y_o; in our case this was not necessary. Depending on the particular problem,values between 0.013 and 0.014 were obtained.

3.3.2. The pressure applied at the outer edge of the inviscid upper layer downstream of the shock wave

The perturbation pressure along the outer edge of the inviscid layer in front of the shock wave has been taken, similarly to Ref. 1, as a constant, namely

$$p'(x,1) = p'(-L,1) = \left\{\frac{2 + (\gamma - 1)\, M^2(-L,1)}{\gamma + 1}\right\}^{-\frac{\gamma}{\gamma-1}} - 1 \qquad (26)$$

Immediately downstream of the shock we then have

$$p'(x_o,1) = \left\{\frac{2 + (\gamma - 1)\, M^2(-L,1)}{\gamma + 1}\right\}^{-\frac{\gamma}{\gamma-1}} \frac{2\gamma M^2(-L,1) - (\gamma - 1)}{\gamma + 1} - 1 \qquad (27)$$

Since the AFEP subroutine for differentiation resembles central differencing, it appears to give some difficulties in crossing the shock wave in only one step, the pressure jump has been applied in three steps, see Fig. 7. The corresponding values for φ used for the differencing of eq. (6) are

$$\varphi(x,1) = - \frac{1}{\gamma}\, p'(-L,1)\, (x + L) \quad , \quad \text{for} \quad -x_o \leq x \leq -\frac{x_o}{2} \qquad (28)$$

$$\varphi(x,1) = \frac{1}{\gamma}\left[\left\{p'(-L,1) - p'(x_o,1)\right\}\frac{x^2}{2x_o} - \left\{p'(-L,1) + p'(x_o,1)\right\}\frac{x}{2} + \left\{p'(-L,1) - p'(x_o,1)\right\}\frac{x_o}{8} - p'(-L,1)\, L\right],$$

$$\text{for} \quad -\frac{x_o}{2} \leq x \leq \frac{x_o}{2} \qquad (29)$$

and

$$\varphi(x,1) = -\frac{1}{\gamma}\left[p'(x_o,1)\ x + p'(-L,1)\ L\right], \quad \text{for } \frac{x_o}{2} \leq x \leq x_o \qquad (30)$$

Due to the very small value of x_o the pressure jump is almost discontinuous.

The pressure at the outer edge of the inviscid layer further downstream of the shock is computed using eqs. (17), (18) and (19), where x has been replaced by $x - x_o$. Downstream from the third meshpoint, being the point situated the closest to the minimum in the after expansion region, a linear pressure distribution is applied until at x = L the pressure recovery is 90% of its value just over the shock wave.

The pressure applied at the outer edge of the inviscid layer downstream of the shock requires a known flow field of the inviscid upper layer. Therefore this flow problem has also been treated iteratively; the first iteration sweep has been performed for a constant pressure, according to eq. (27).

The free parameter s_{10} in eq. (17) has taken into account by assuming (in all iteration sweeps but the first)

$$p'(x_{i3},1) = \frac{1}{3}\,p'(-x_o,1) + \frac{2}{3}\,p'(x_o,1) \qquad (31)$$

where x_{i3} is the third meshpoint after x = x, mentioned above. The assumption made in eq. (31) involved that in the iteration process, $p'(x,1)$ only changes in the region $x_o \leq x \leq x_{i3}$. The expression has been chosen since it appeared to give reasonable good agreement to the experiments of Refs. 2 and 7; if necessary, other matching values obtained from the inviscid outer flow field could be introduced.

3.4. Computation of perturbation pressure and perturbation velocity

In all meshpoints of the inviscid upper layer p' and v' are determined from eq. (6) using the standard subroutines for differentiation of the AFEP package. Eq. (2) is integrated with respect to x, knowing the incoming velocity profile at x = -L given by eq. (20), this yields u'

$$u'(x,y) = -\frac{1}{\gamma}\frac{M_o^*(y)}{M_o^{2}(y)}\,p'(x,y) - \frac{1}{M_o^*(y)}\,\frac{\ell}{\delta}\,\frac{dM_o^*(y)}{dy}\int_{-L}^{x} v'(\xi.y)\,d\xi$$

$$+ M^*(-L,1)\left[1 + \frac{1}{K}\sqrt{\frac{c_f(-L)}{2}\left\{1 + r\,\frac{\gamma-1}{2}\,M^2(-L,1)\right\}}\ .\right.$$

$$\left.\left.\cdot\left\{\ln y - 0{,}5\ (1 + \cos \pi y)\right\}\right] +$$

$$- M_o^*(y) + \frac{1}{\gamma} \frac{1}{M_o(y)} \sqrt{\frac{\gamma + 1}{2 + (\gamma - 1)\, M_o^2(y)}}\, p'(-L,y) \qquad (32)$$

In eq. (32) the integral has been replaced by a Riemann-sum.

That the flow in the viscous sublayer cannot be considered as an incompressible flow follows from the computed Mach number at $y = y_o$, the edge of the sublayer. For $y_o = 0.01$, $M(-L,1) = 1.3$ and $c_f(-L) = 0.002$; $M(-L,y_o) = 0.6241$.

The perturbation pressure p' in the viscous sublayer is obtained from $p' = p'(x,y_o)$, which is known from the inviscid upper layer for an established value of y_o (see 3.3.1.), since $\partial p'/\partial y$ in the sublayer is assumed (Ref. 1) to be zero.
The horizontal perturbation velocity u' in the sublayer is computed with eq. (16), knowing $p'(x,y_o)$ and $u'(x,y_o)$.
The vertical perturbation velocity $v' = 0$, which, again, is an assumption made in the flow model of Ref. 1.

4. RESULTS

4.1. Test cases

The numerical results of the present method (labeled: present results) are compared with some experimental data: Ackeret, Feldmann and Rott (Ref. 2, labeled: A.F. & R.) and Gadd (Ref. 7, labeled: Gadd).
The experiments of Ref. 2 have been made on a convex surface ($R \approx 0.5$ m) and those of Ref. 7 are carried out on a plane wall.
Test cases were:

A.F. & R.:	1.	$M = 1.3225$,	$Re = 2.63 \cdot 10^6$	Fig. 8
	2.	$M = 1.1897$,	$Re = 2.658 \cdot 10^6$	Fig. 9
	3.	$M = 1.2618$,	$Re = 2.692 \cdot 10^6$	Fig. 10
	4.	$M = 1.3121$,	$Re = 2.683 \cdot 10^6$	Fig. 11
Gadd :	5.	$M = 1.12$,	$Re = 6.0 \cdot 10^6$	Fig. 12
	6.	$M = 1.15$,	$Re = 7.0 \cdot 10^6$	Fig. 13
	7.	$M = 1.27$,	$Re = 10.0 \cdot 10^6$	Fig. 14
	8.	$M = 1.34$,	$Re = 19.3 \cdot 10^6$	Fig. 15

M is the Mach number at the edge of the boundary layer just ahead of the shock wave, and Re is the Reynolds number based on a characteristic length. In Ref. 2 this length is taken as the length of the convex plate where the experiments are made and in Ref. 7 it is the length where the boundary layer develops in front of the shock wave.

4.2. Surface pressure distributions

All numerical surface pressure distributions of Figs. 8-15 show a steeper pressure rise than the experimental pressure distributions. This may be due to the implementation of the Bohning-Zierep model at the edge of the inviscid sublayer and due to the virtual absence of viscosity and of turbulence in the two layer system.
The analytical model of Bohning and Zierep (Fig. 8) shows an even steeper pressure rise since their pressure jump at the edge is discontinuous, whereas in the present case it consists in three steps (Fig. 7).

A difficulty occurred in plotting the numerical results as compared to the experiments; it was not possible to determine accurately the experimental shock wave position. Bohning and Zierep apparently have chosen this position somewhat more downstream than we have done in the present case. For equal shock wave position the curves of the present numerical results and of the analytical Bohning-Zierep model (Ref. 8) practically coincide.
The results of Messiter (Ref. 9) are only available downstream of the shock (Fig. 8).
In Fig. 12 the pressure distribution is compared to the experimental results of Gadd (Ref. 7) and to some (prominent) theoretical distributions (Refs. 9, 10, 11). It should be mentioned that the theoretical pressures of Inger and Mason (Ref. 10) and of Messiter (Ref. 9) are in a better agreement with the initial pressure rise than the present results. Probably their model description is somewhat closer to the real viscous flow behaviour.

4.3. Pressure distribution in the inviscid upper layer

Figs. 16 and 17 represent the outsmearing of the applied steep pressure jump at the edge of the layer, into the layer towards the wall. Applying eq. (31) in order to match the outer flow conditions, means that the magnitude of the after expansion is unaffected by the streamline curvature at the foot of the shock wave. This fact contradicts of course the Oswatitsch-Zierep conjecture that this curvature should influence the amount of expansion behind the shock wave. However, the relation (31) is obtained by taking into account the measurements of Ref. 2 and 7. It is not unlikely that a different behaviour of the after expansion at the foot of the shock wave than that given by the Oswatitsch-Zierep model (for instance a less steep after-expansion) might affect the slope of the pressure distribution at the wall.
It might be worthwhile to subject the two-layer boundary layer model of Bohning and Zierep to such a new extern flow field.

4.4. Velocity profiles

The velocity profiles are plotted in Figs. 18 and 19. There appears quite a disagreement between the profiles of the experiments in Ref. 2 and the present numerical results (Fig. 18). The agreement is reasonable in Fig. 19 where the present results are compared with the experiments of Ref. 7. The reason for the difference may be sought in the much lower Mach number of the latter case. Since the Bohning-Zierep model is based on disturbance of a $M = 1$ basic flow a better result may be expected for a Mach number closer to unity. Another reason for the disagreement in test case 1 may be the difficulty of finding a suitable incoming velocity profile at $x = -L$ since in the experiments of Ref. 2 there is no profile given at that position. In addition there is some doubt about the flow attachment in the test case 1 experiments.

Serious doubt exists where the numerical results show a reverse flow. The flow model is not suitable for such a phenomenon, since the hypothesis of "perturbation of a basic flow" is violated. However, it might indicate that the flow model breaks down and one has to look for a different approach, as Bohning and Zierep do in Ref. 12.

Figs. 20 and 21 show the position of the sonic line with respect to x, i.e. with respect to the distance along the wall made non-dimensional with the boundary layer thickness. The course of the sonic line shows the same behaviour as in the Bohning and Zierep solution (Ref. 1). From $x = -1$ downstream it runs towards $y = 1$ at $x = 0$.

4.5. Distribution of the vertical velocity component

From Figs. 22 and 23 it may be seen that the entire inviscid upper layer has an upwash, which increases with increasing distance from the wall, accumulating into a peak at the foot of the shock wave. Such a peak not only involves an oblique shock wave, but also a kinked streamline. These features have not been taken into account in the initial boundary conditions. For instance the pressure jump through the shock wave was taken using normal shock relations. This could be argumented by the results for v, because $v \ll u$.

Another more severe restriction, also occurring in the analytical results of Ref. 1, is the fact that an oblique shock does not have a singularity at its foot. There is, however, always the possibility of an after-expansion that is regular in the sense that the streamline behaviour behind the shock is convex, as shows the v-distribution in Figs. 22 and 23. It would be interesting to change the flow model such that instead of the Oswatitsch-Zierep singularity a regular expansion wave is applied as for instance Inger suggests (Ref. 13).

The results in Figs. 22 and 23 are asymmetric with respect to $x = 0$. According as one goes deeper into the boundary layer the point of maximum upwash moves upstream.

At $y = y_o$, the edge of the viscous sublayer, v should be 0 as the boundary condition there states. A drawback of the used AFEP computation procedure is that the Neumann conditions are better satisfied when the meshwidth in vertical direction is decreased in the vicinity of the boundary. In the present computercode we have not tried the utmost.

At $x = \pm 1$ the vertical velocity component is practically zero (0.00005), suggesting that the original Bohning and Zierep assumption to confine the problem on the interval $-1 \leq x \leq 1$ is good enough.

4.6. Streamline distribution

The streamlines shown in Figs. 24 and 25 are computed by integrating the flow directions, or rather by following the flow directions from point to point, knowing the velocity components. Only those streamlines are computed which remain within the inviscid upper layer on the interval $-0.2 \leq x \leq 0.2$. In test case 1 this is the streamline entering at $x = -0.2$ at $y = 0.967$ and in test case 5 it is the streamline at $y = 0.986$.

5. CONCLUDING REMARKS

- The implementation of the Bohning and Zierep model (Ref. 1) into a numerical treatment of the shock wave-boundary layer interaction problem appears to deliver a better tool for the description, and, taking into account the larger applicable variety of flow parameters, a more powerfull method than the analytical treatment given in Ref. 1.
  In addition a numerical method does not seem to be more complicated, since the use of hypergeometric functions, often involved in analytic transonic flow problems, is rather difficult also.
- The agreement of the method with existing theories and with experiments is reasonable, although the agreement between theoretical results is better than with experiments. This may be due to the insufficient viscous modelling not to speak about the modelling of the turbulence.
- There is a problem in the Bohning and Zierep approach in that the initial normal shock wave becomes oblique during the numerical development of the flow as it iterates to the final solution.
  As a consequence the Oswatitsch-Zierep singularity vanishes and so does the accompanying after-expansion. However, also oblique shock waves can be succeeded by expansion regions, therefore it would be interesting to apply from the beginning such an outer flow and take, as a first guess, a curved, or even kinked, streamline at the foot of the shock. Such a starting point may throw some light on the point of the good agreement between the results of the present method and the experimental results for plane walls (Gadd, Ref. 7), since the oblique shock-after expansion flow also occurs at plane walls. The diffusion of such an initial expansion would be worthwhile to compare with the results obtained by the normal shock wave model of Oswatitsch-Zierep.
- If the outer flow field is known and the shock wave-boundary layer interaction is not that severe that it causes flow separation, the Bohning-Zierep model may easily incorporated in numerical codes in order to solve the entire transonic flow problem around aerofoils.

6. REFERENCES

1. Bohning, R. and J. Zierep,
Der senkrechte Verdichtungsstoss an der gekrümmten Wand unter Berücksichtigung der Reibung,
ZAMP 27 (1976), p. 225-240.

2. Ackeret, J., F. Feldmann and N. Rott,
Untersuchungen an Verdichtungsstössen und Grenzschichten in schnell bewegten Gasen,
Mitteilungen aus dem Institut für Aerodynamik an der E.T.H. Zürich, Nr. 10, 1946.

3. Zierep, J.,
Theorie der Schallnahen und der Hyperschallströmungen,
Verlag G. Braun, Karlsruhe, 1966.

4. Segal, A.,
AFEP User Manual,
Dept. of Mathematics and Informatics, Delft University of Technology, Delft, 1981.

5. Segal, A.,
AFEP Standard Elements,
Dept. of Mathematics and Informatics, Delft University of Technology, Delft, 1981.

6. Segal, A.,
AFEP Programmers Guide,
Dept. of Mathematics and Informatics, Delft University of Technology, Delft, 1981.

7. Gadd, G.E.,
Interactions Between Normal Shock Waves and Turbulent Boundary Layers,
Aeronautical Research Council, London, R & M 3262, 1962.

8. Bohning, R. and J. Zierep,
Normal Shock - Turbulent Boundary Layer Interaction at a Curved Wall,
AGARD-CP-291, 1980.

9. Messiter, A.F.,
Interaction Between a Normal Shock Wave and a Turbulent Boundary Layer at High Transonic Speeds, Part I: Pressure Distribution,
ZAMP 31 (1980), p. 204-226.

10. Inger, G.R. and W.H. Mason,
Analytical Theory of Transonic Normal Shock Turbulent Boundary Layer Interaction,
AIAA Journal Vol. 14 (1976), p. 1266-1272.

11. Melnik, R.E. and B. Grossman,
Analysis of the Interaction of a Weak Normal Shock Wave with a Turbulent Boundary Layer,
AIAA Paper, No. 74-598, 1974.

12. Bohning, R. and J. Zierep,
Bedingung für das Einsetzen der Ablösung der turbulenten Grenzschicht an der gekrümmten Wand mit senkrechtem Verdichtungsstoss,
ZAMP 29 (1878), p. 190-198.

13. Inger, G.R.,
Transonic Shock-Turbulent Boundary Layer Interaction and Incipient Separation on Curved Surfaces,
AIAA Paper, No. 81-1244, 1981.

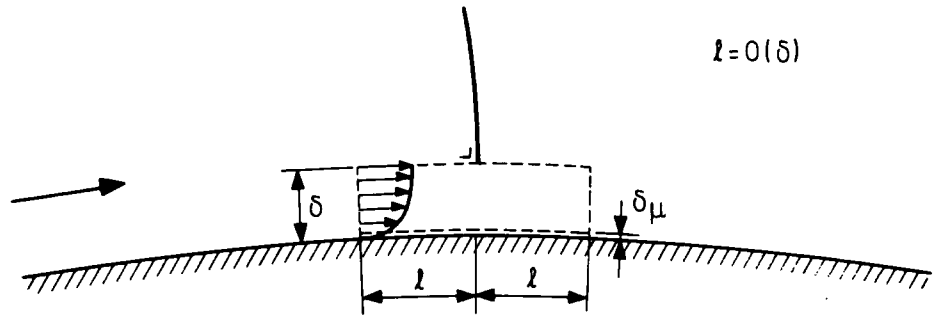

Fig. 1 : Region of interaction in the Bohning-Zierep model.

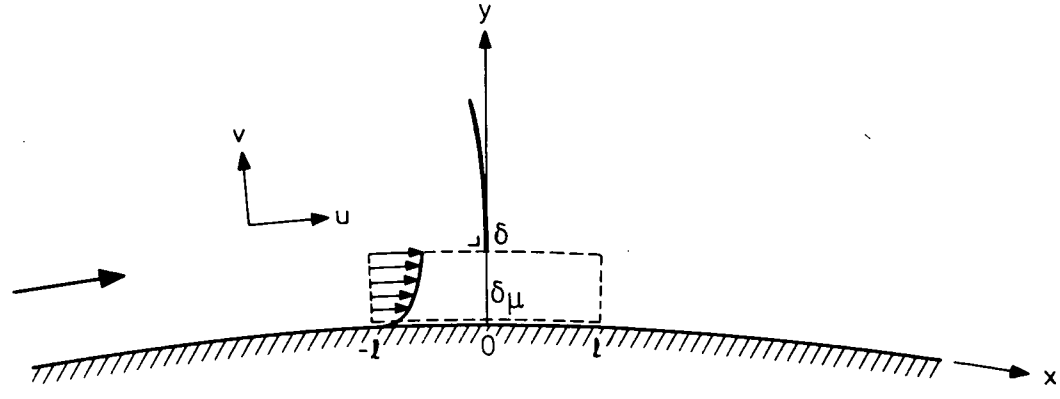

Fig. 2 : Coordinate system and velocity components.

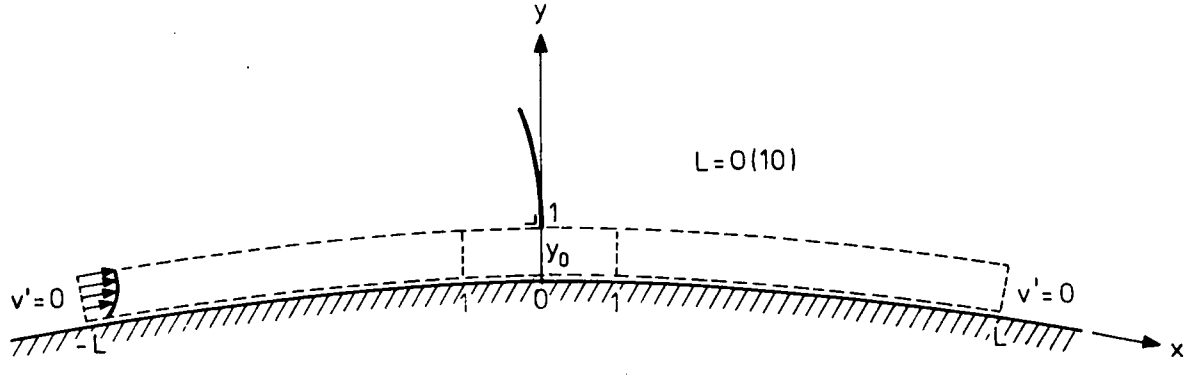

Fig. 3 : Region of integration.

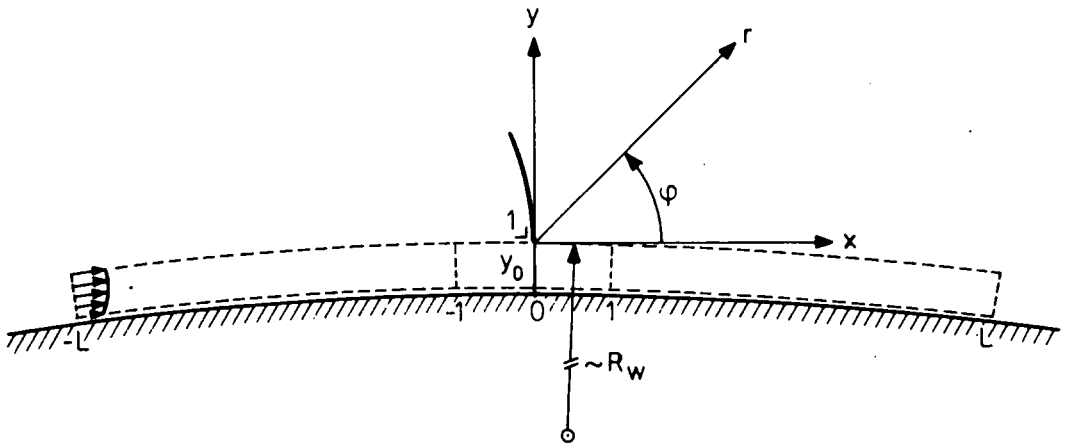

Fig.4 : Coordinate systems used for the application of the Oswatitsch-Zierep shock wave (Ref. 7).

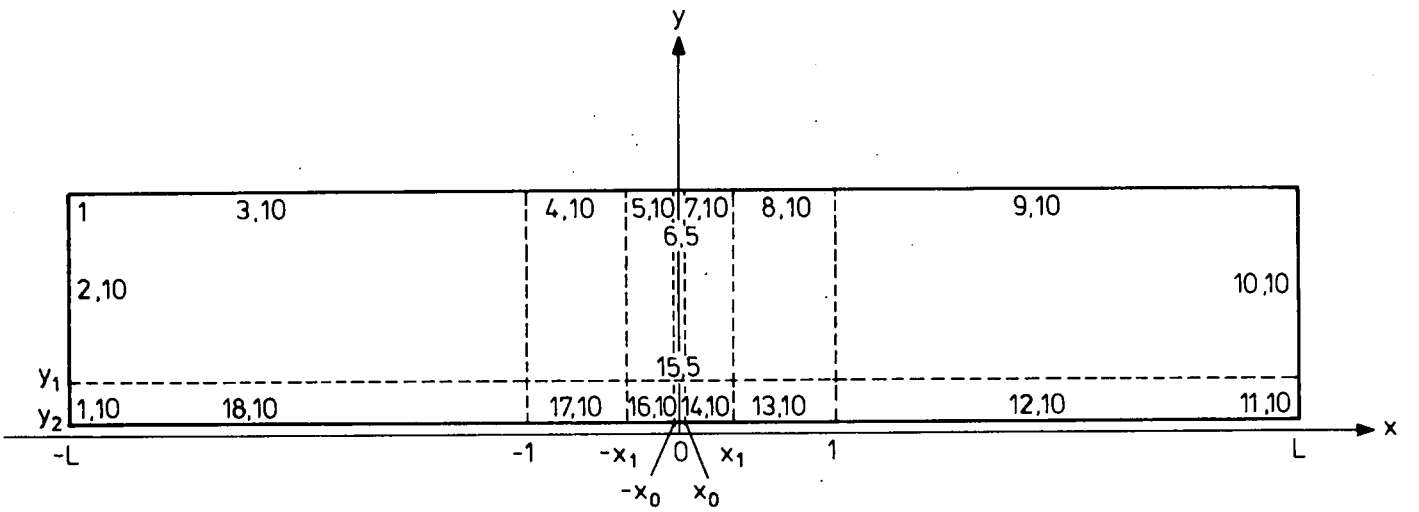

Fig. 5 : Distribution of meshpoints in the computational program.

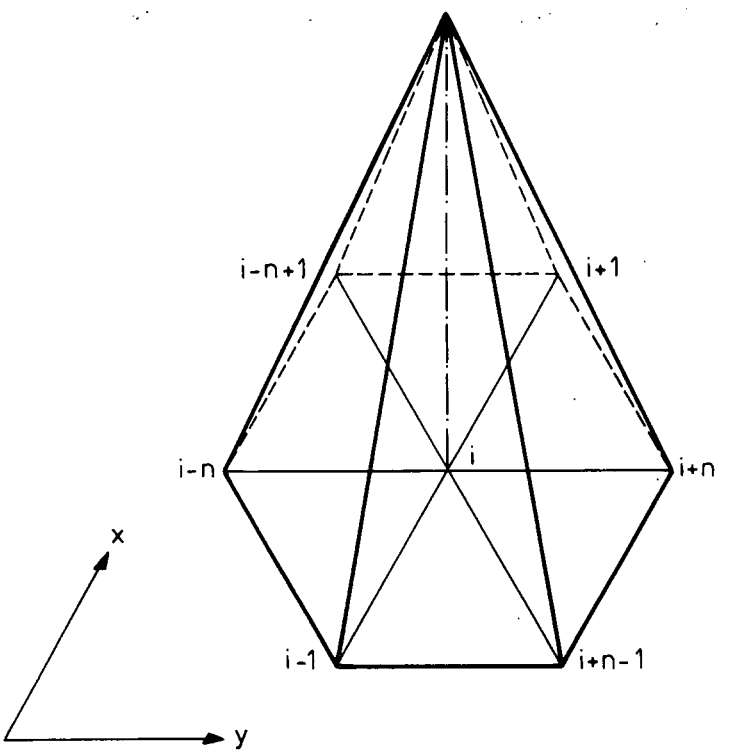

Fig. 6 : Representation of a linear elementary function $f_i(x,y)$.

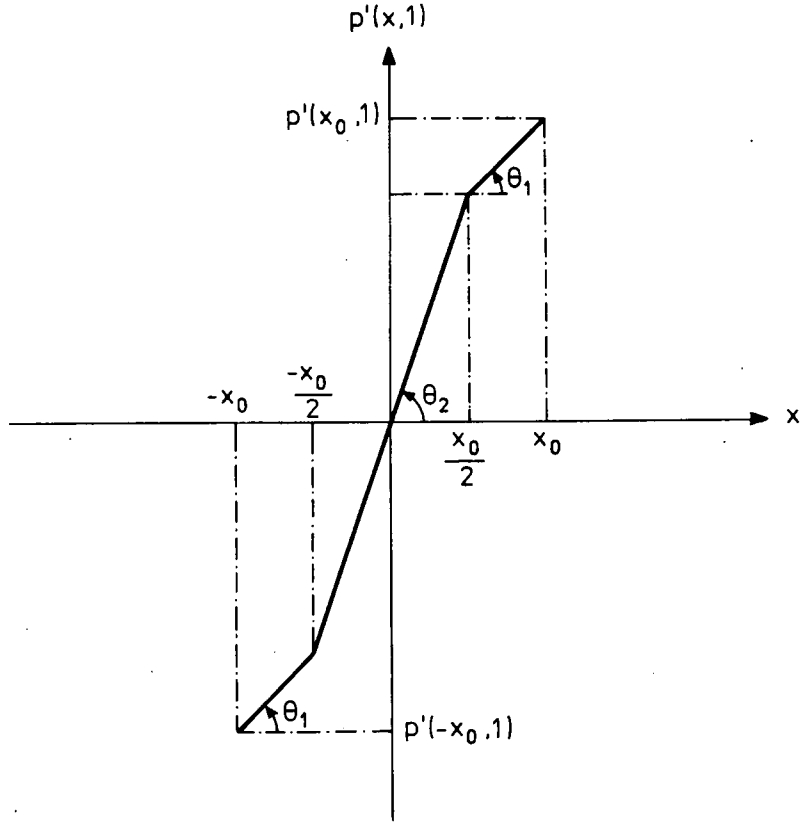

Fig. 7 : Simulation of pressure rise across the shock wave.

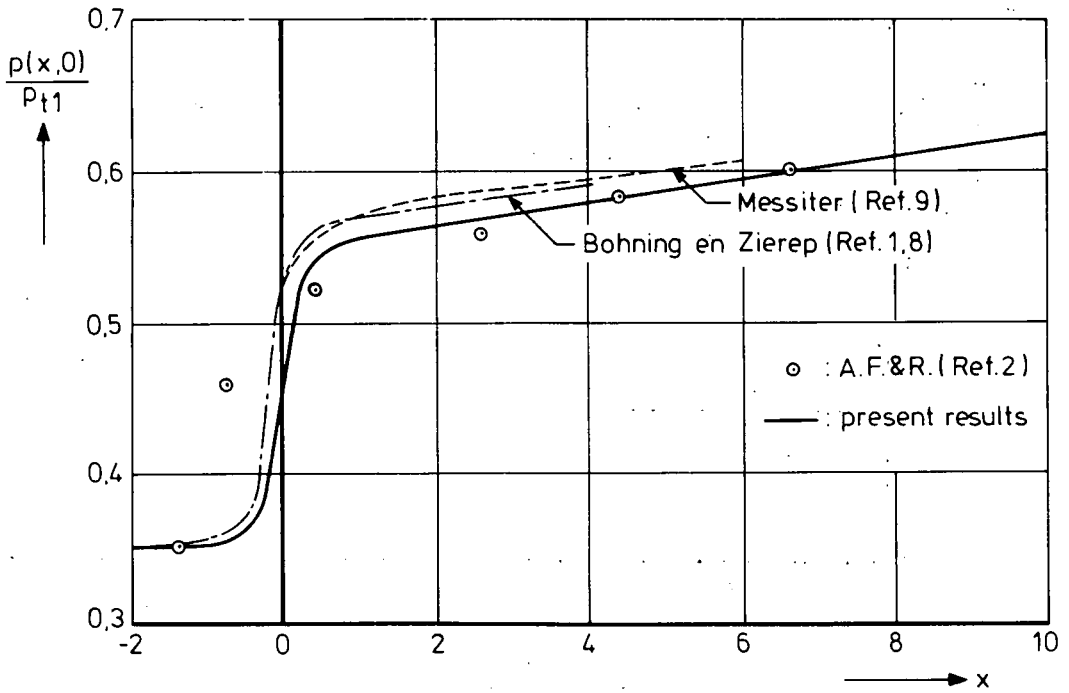

Fig. 8 : Surface pressure distribution ; test case 1 :
M = 1.3225 , Re = $2.63 \cdot 10^6$.

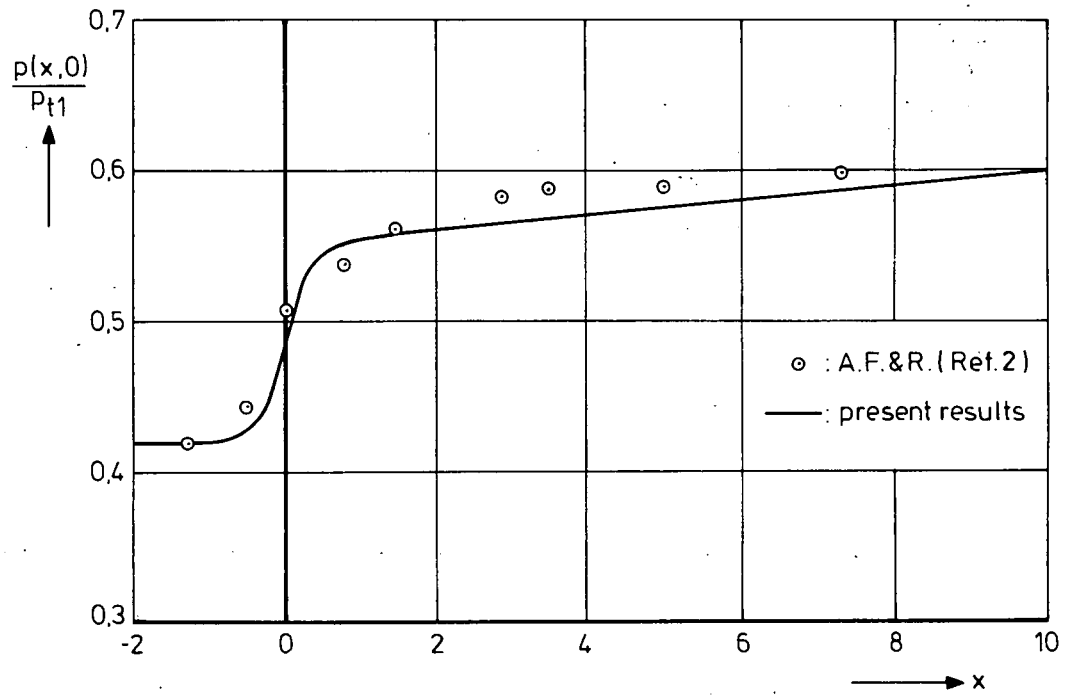

Fig. 9 : Surface pressure distribution ; test case 2 :
M = 1.1897 , Re = $2.658 \cdot 10^6$.

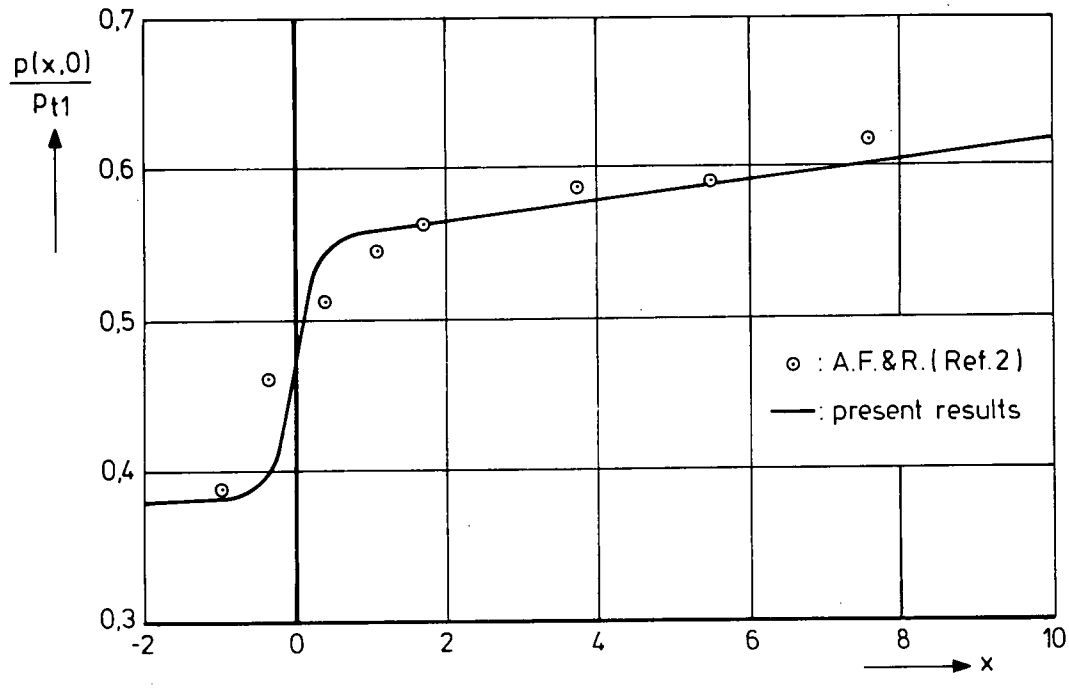

Fig. 10 : Surface pressure distribution ; test case 3 :
M = 1.2618 , Re = $2.692 \cdot 10^6$.

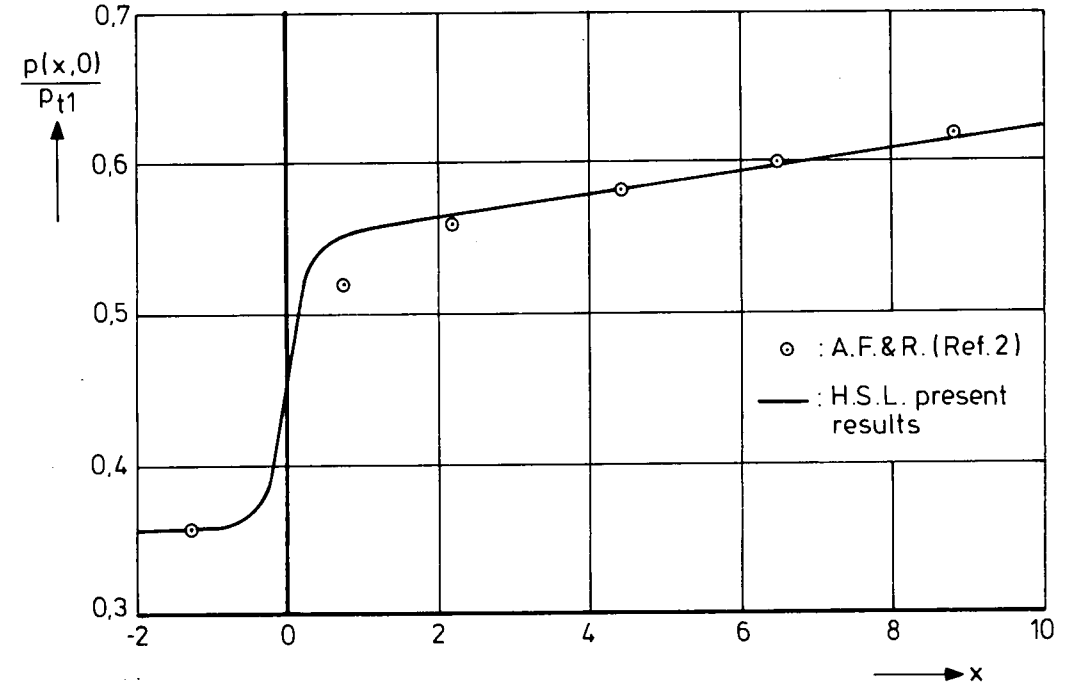

Fig. 11 : Surface pressure distribution ; test case 4 :
M = 1.3121 , Re = $2.683 \cdot 10^6$.

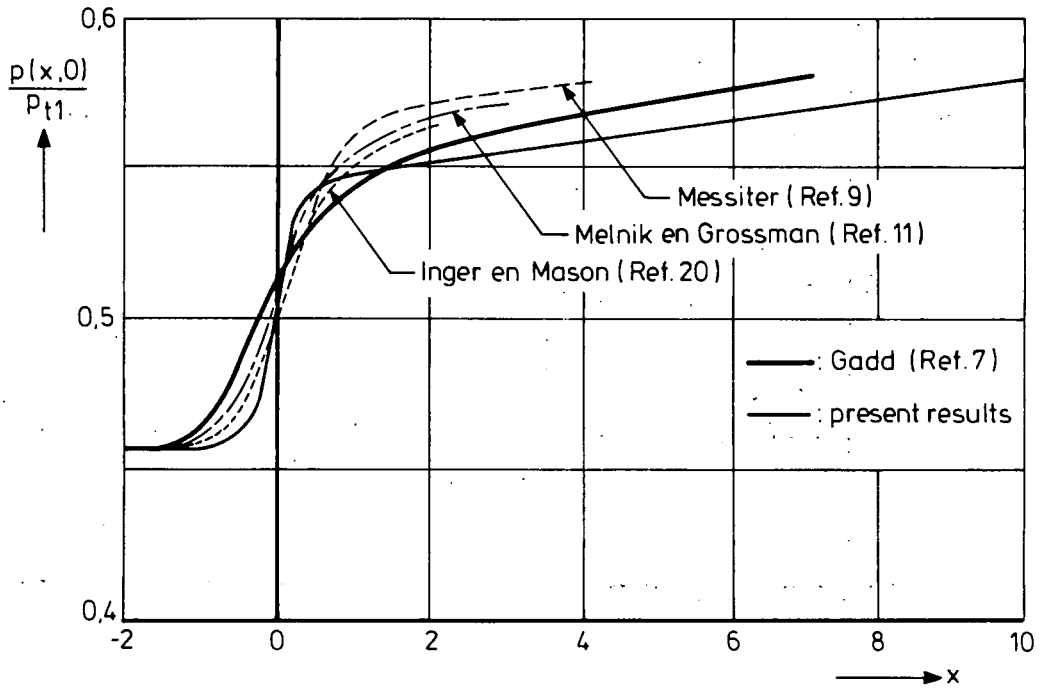

Fig. 12 : Surface pressure distribution ; test case 5 :
$M = 1.12$, $Re = 6.0 \cdot 10^6$.

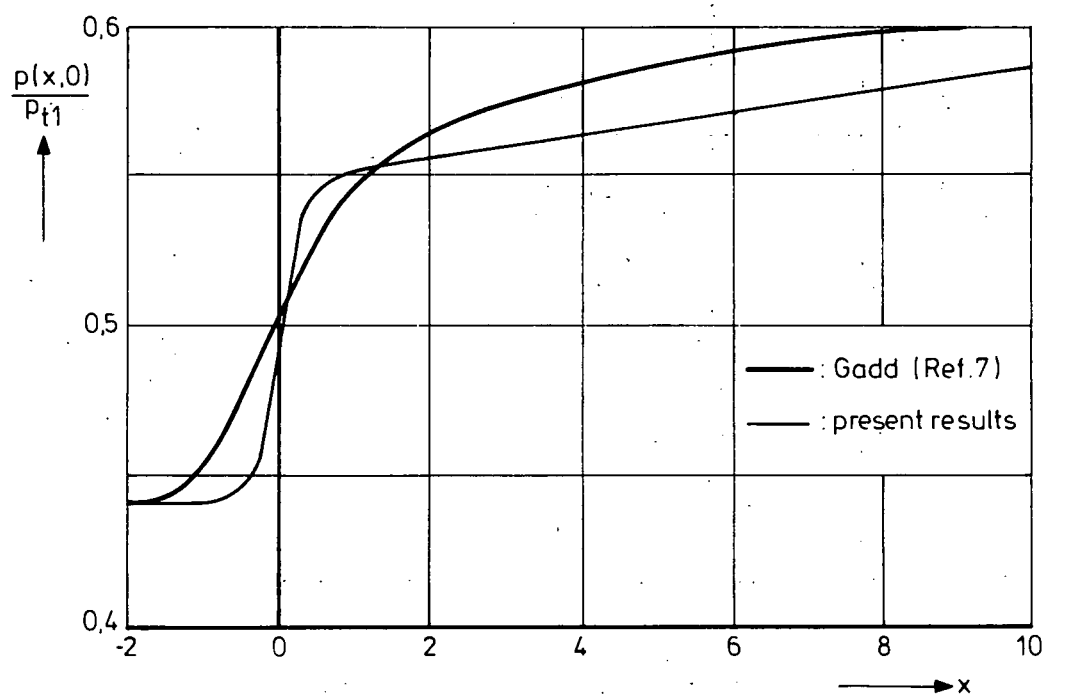

Fig. 13 : Surface pressure distribution ; test case 6 :
$M = 1.15$, $Re = 7.0 \cdot 10^6$.

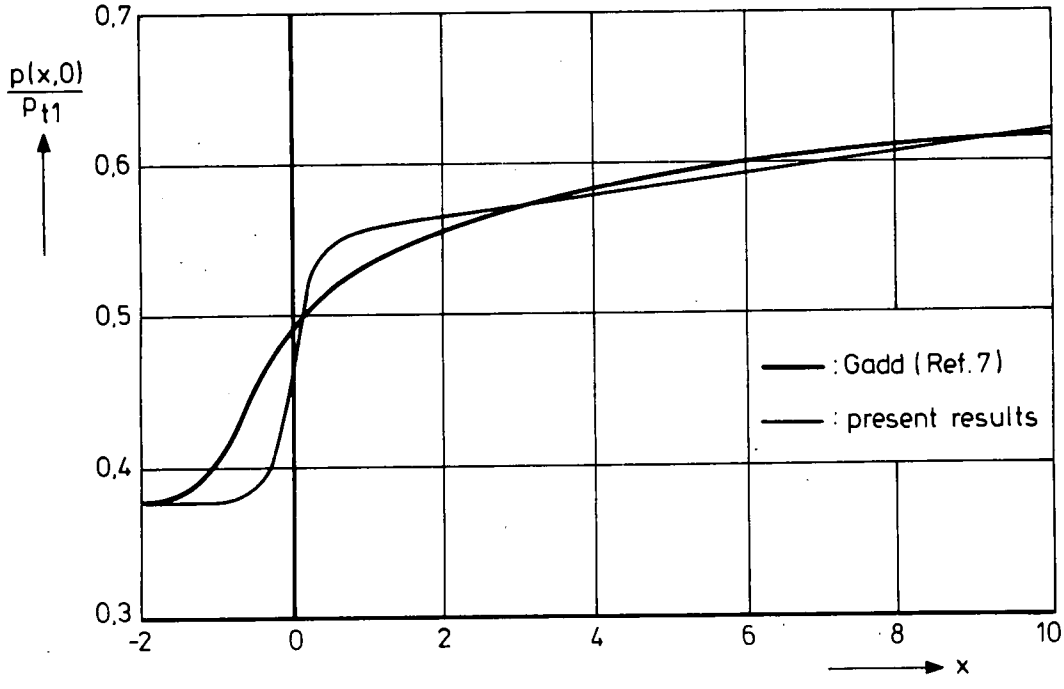

Fig. 14 : Surface pressure distribution ; test case 7 :
M = 1.27, Re = 10.0·10^6.

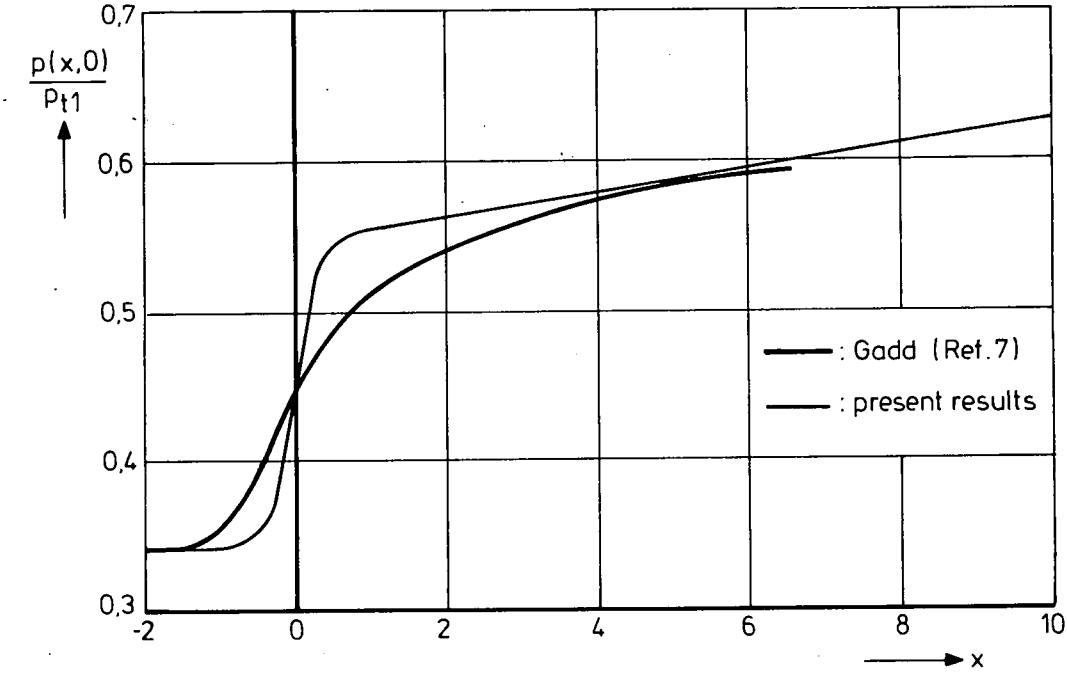

Fig. 15 : Surface pressure distribution ; test case 8 :
M = 1.34, Re = 19.3·10^6.

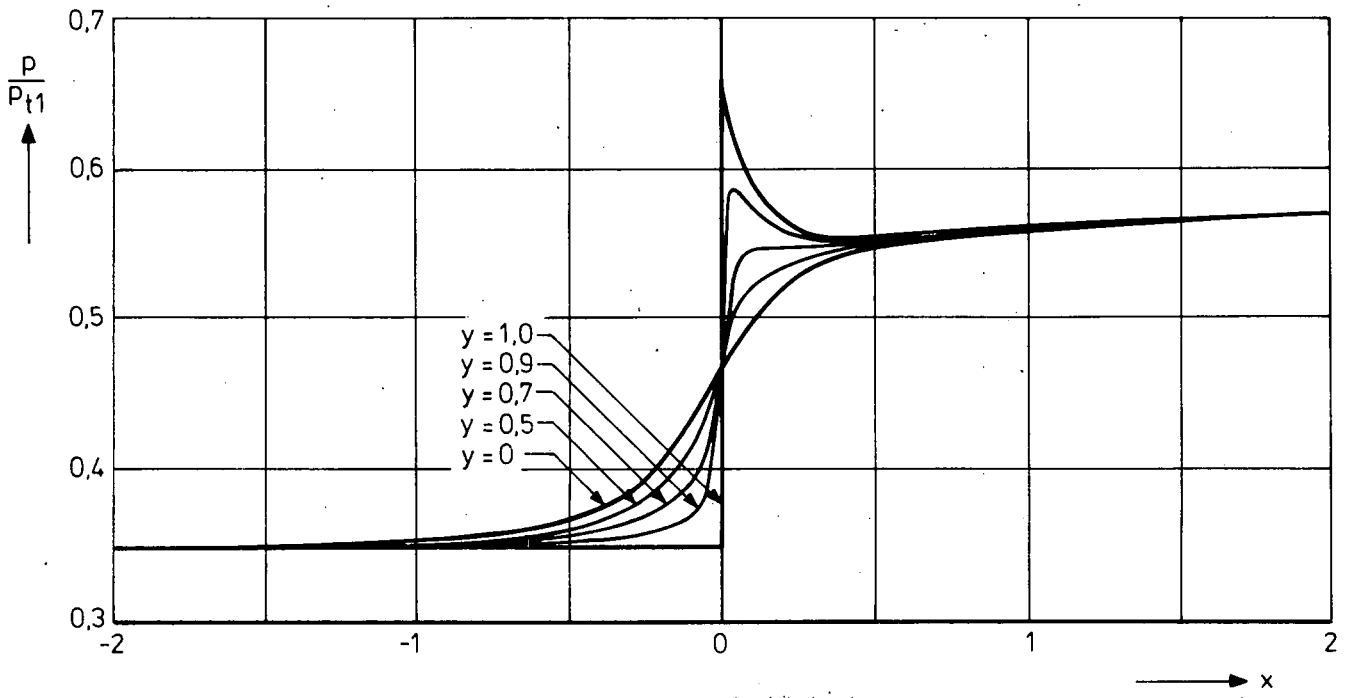

Fig. 16 : Pressure distribution at different levels in the boundary layer ; test case 1 : M = 1.3225 , Re = $2.63 \cdot 10^6$.

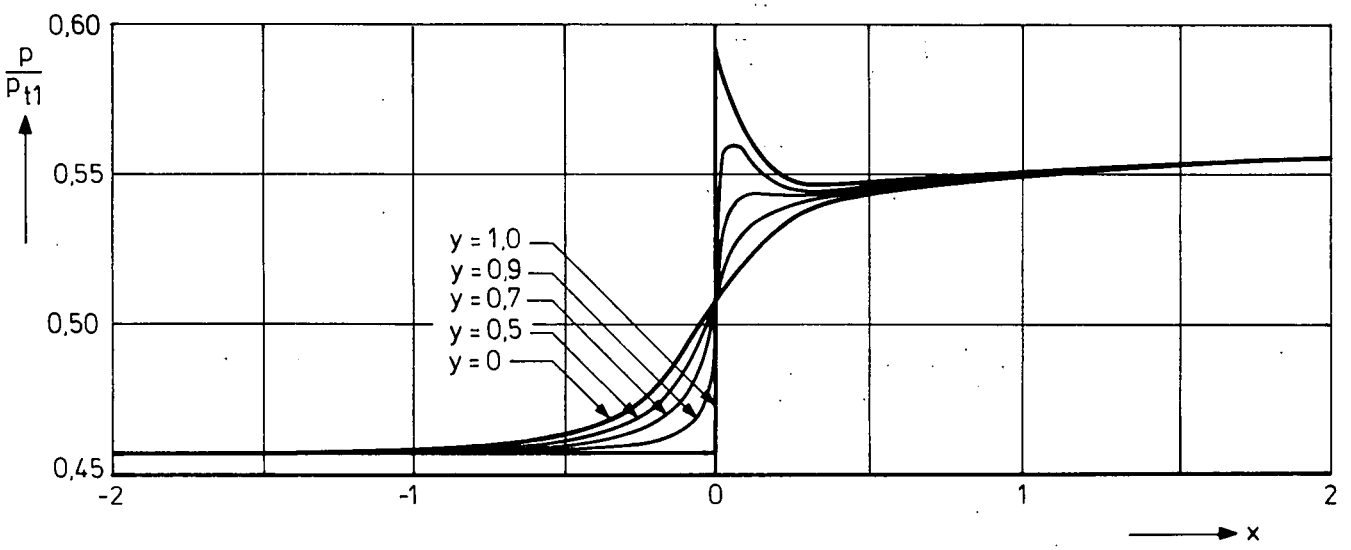

Fig. 17 : Pressure distribution at different levels in the boundary layer ; test case 5 : M = 1.12 , Re = $6.0 \cdot 10^6$.

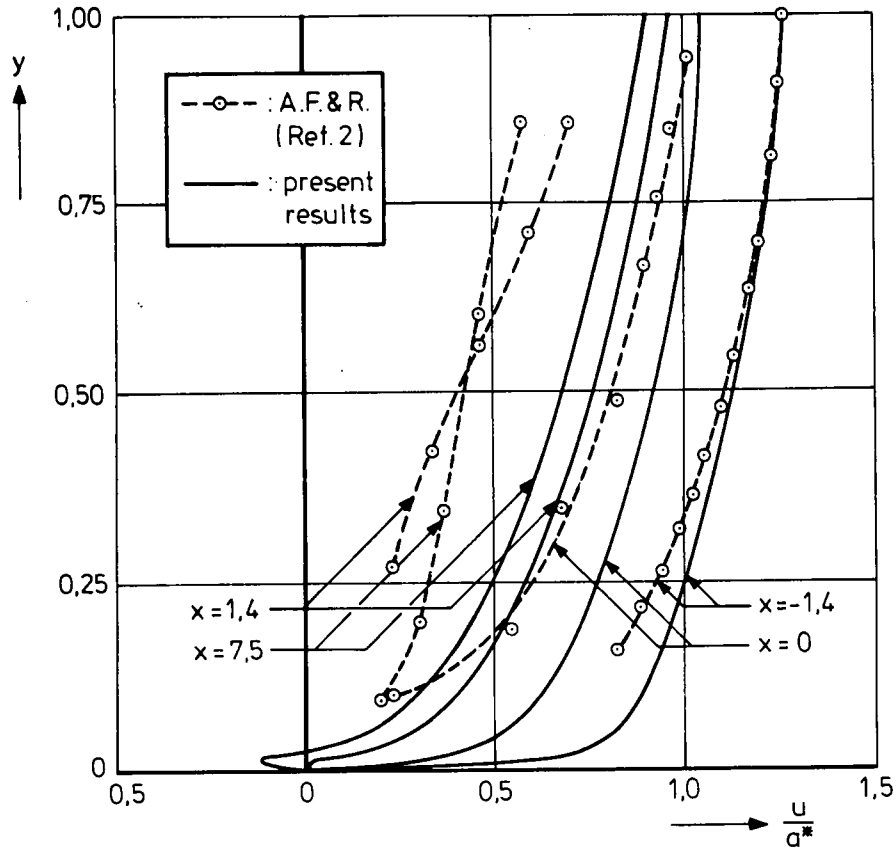

Fig. 18 : Velocity profiles ; test case 1 : M = 1.3225 , Re = $2.63 \cdot 10^6$.

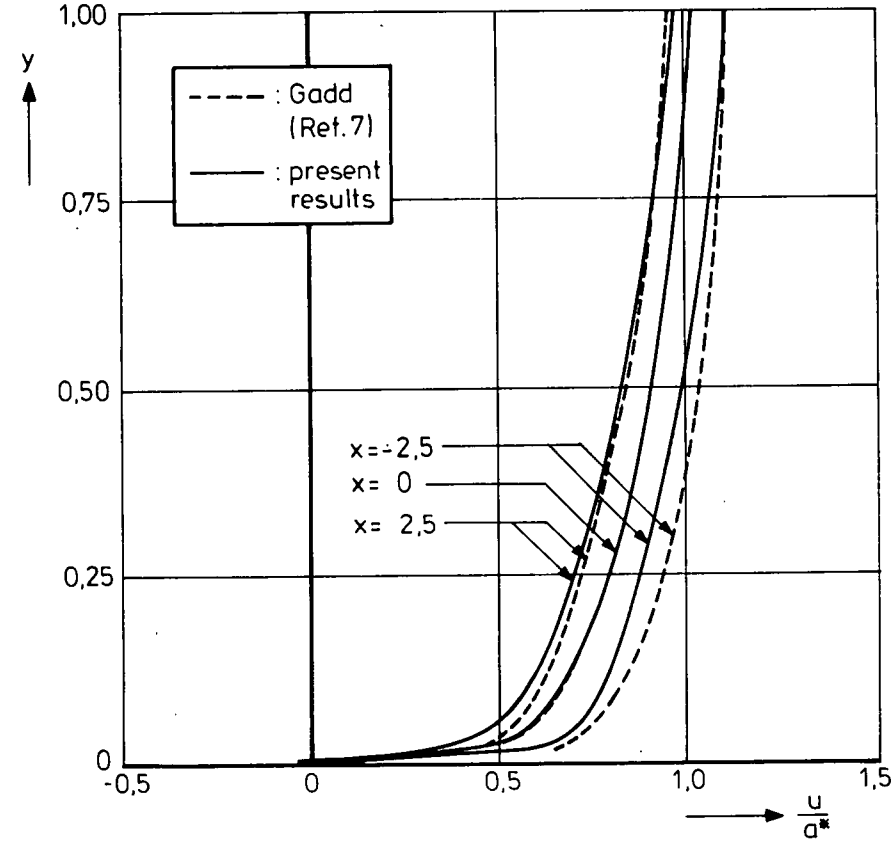

Fig. 19 : Velocity profiles ; test case 5 : M = 1.12 , Re = $6.0 \cdot 10^6$.

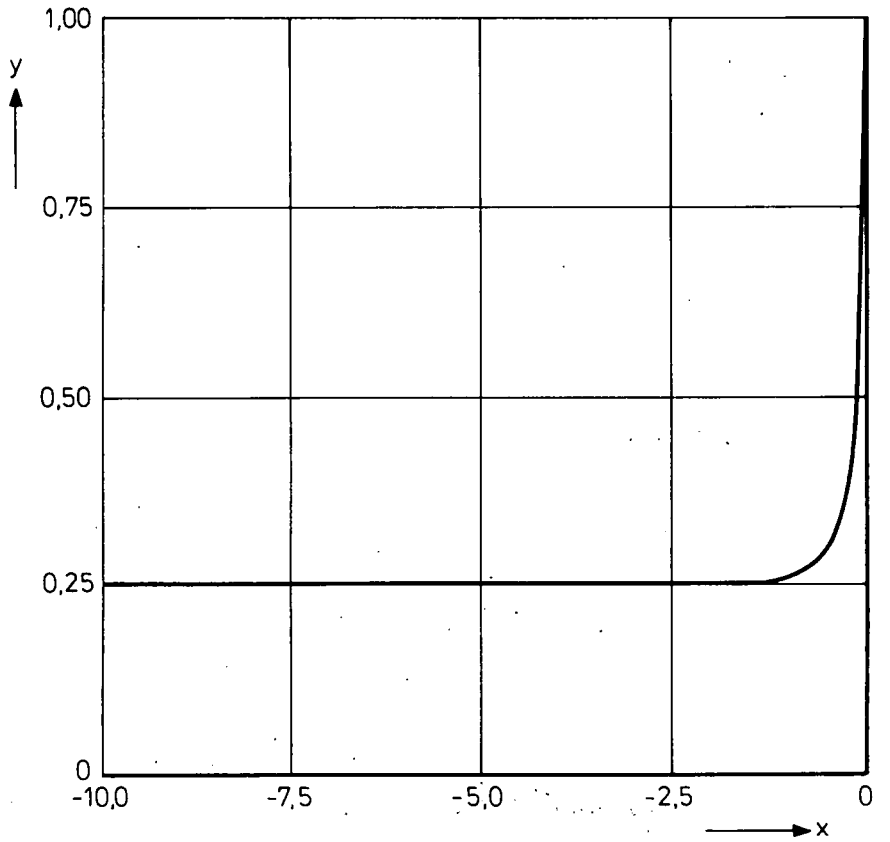

Fig. 20 : Position of the sonic line ; test-case 1 :
M = 1. 3225 , Re = $2.63 \cdot 10^6$.

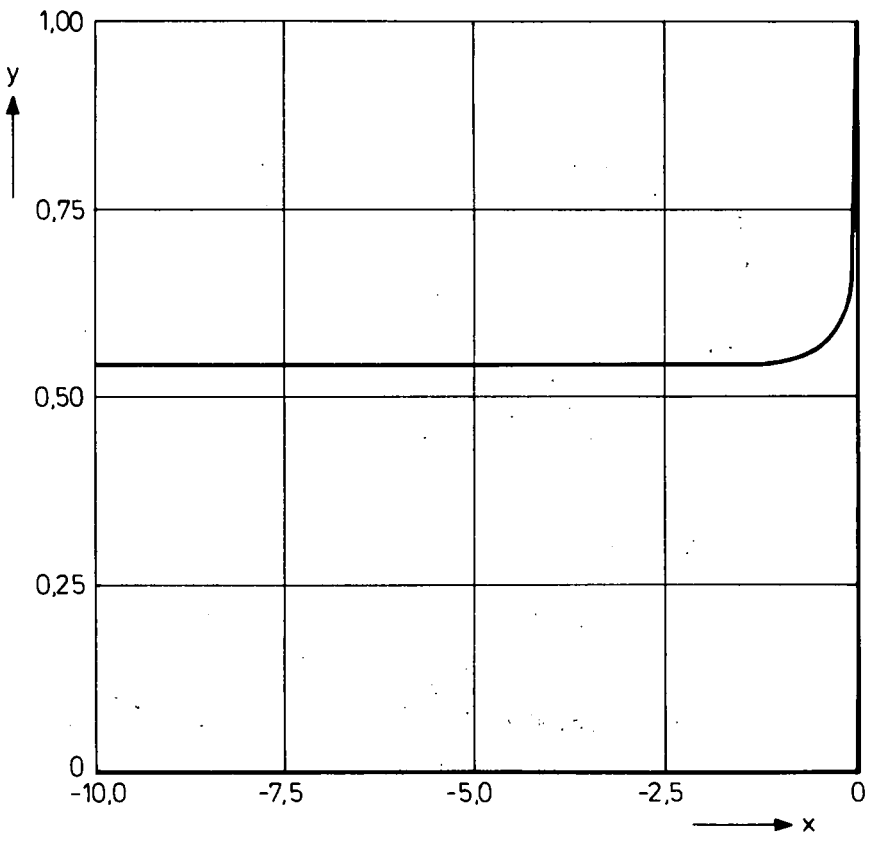

Fig. 21 : Position of the sonic line ; test-case 5 :
M = 1.12 , Re = $6.0 \cdot 10^6$.

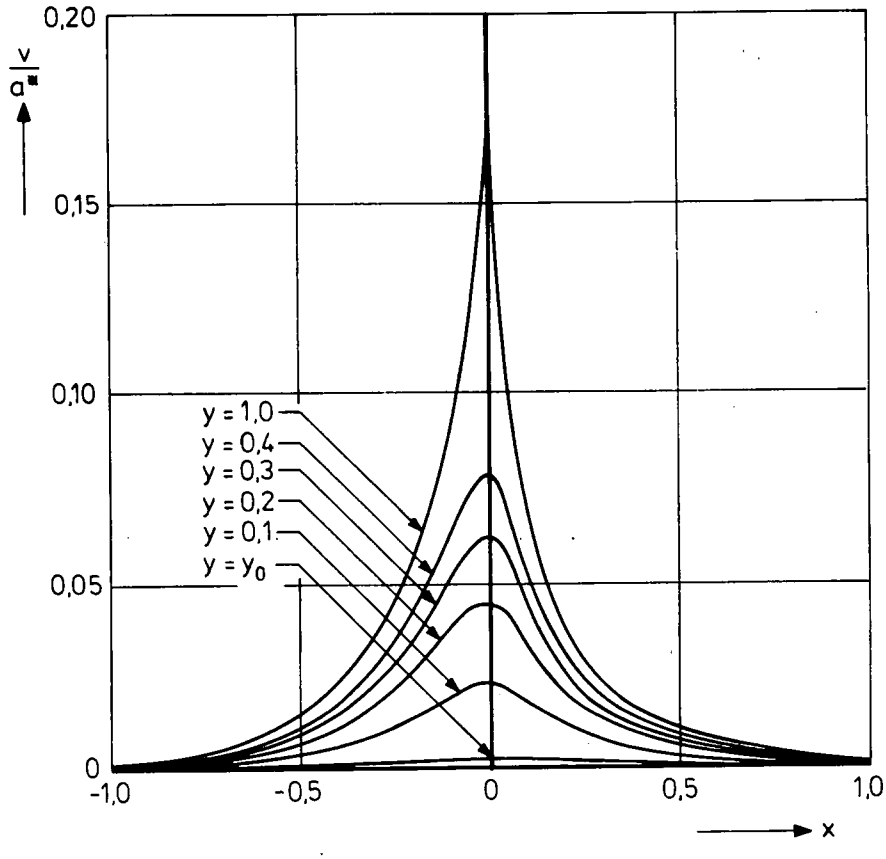

Fig. 22 : Vertical velocity component , test-case 1 :
$M = 1.3225$, $Re = 2.63 \cdot 10^6$.

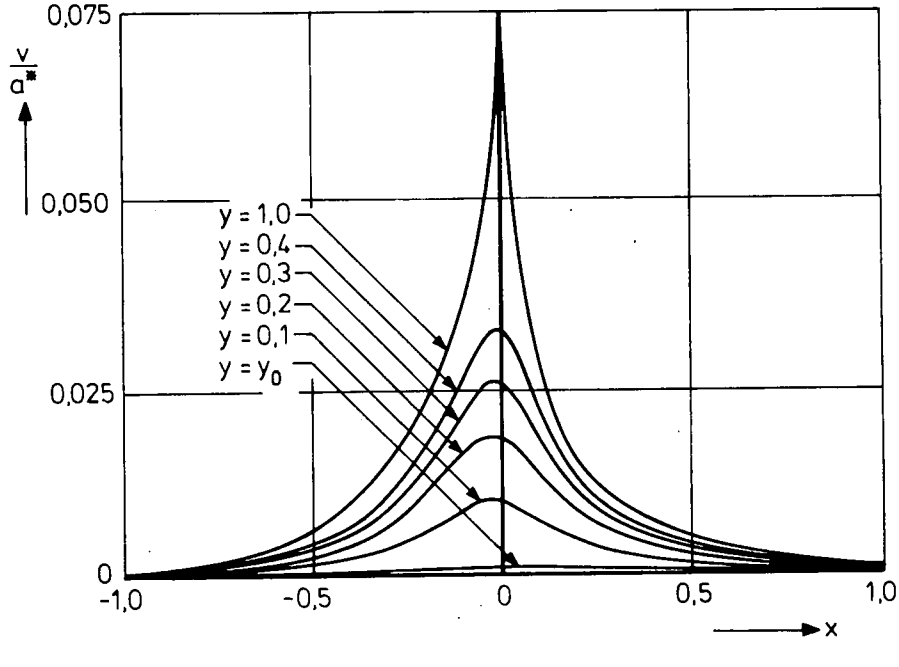

Fig. 23 : Vertical velocity component ; test-case 5 :
$M = 1.12$, $Re = 6.0 \cdot 10^6$.

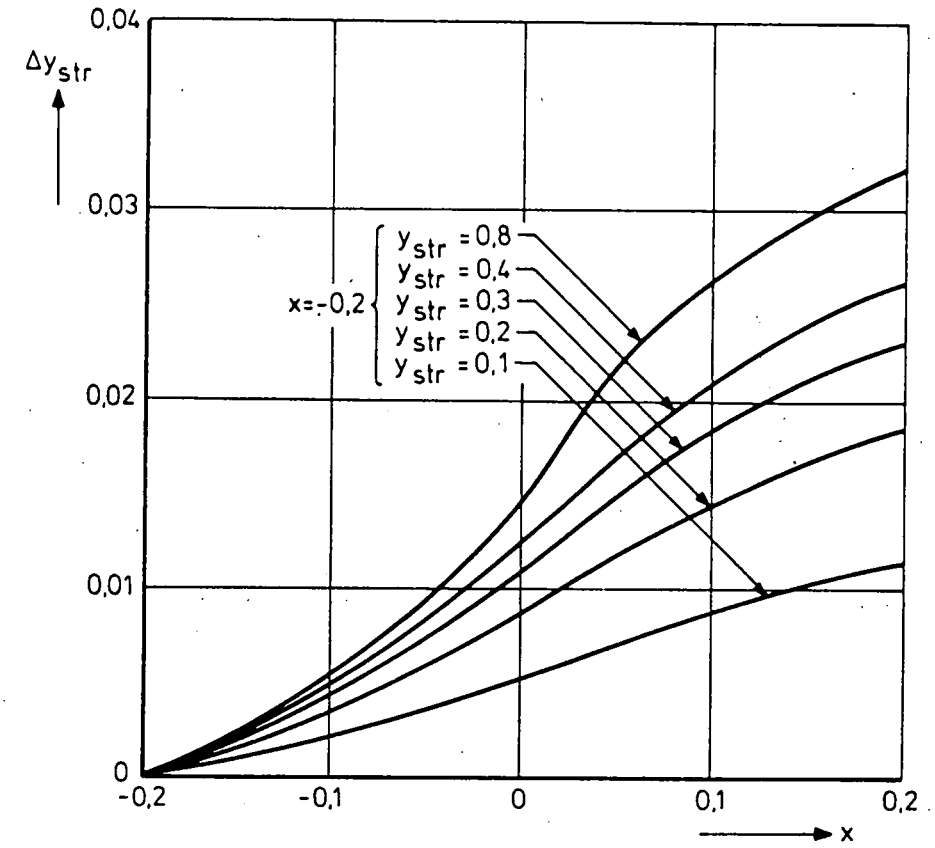

Fig. 24 : Streamlines ; test case 1 : M = 1.3225 , Re = $2.63 \cdot 10^6$.

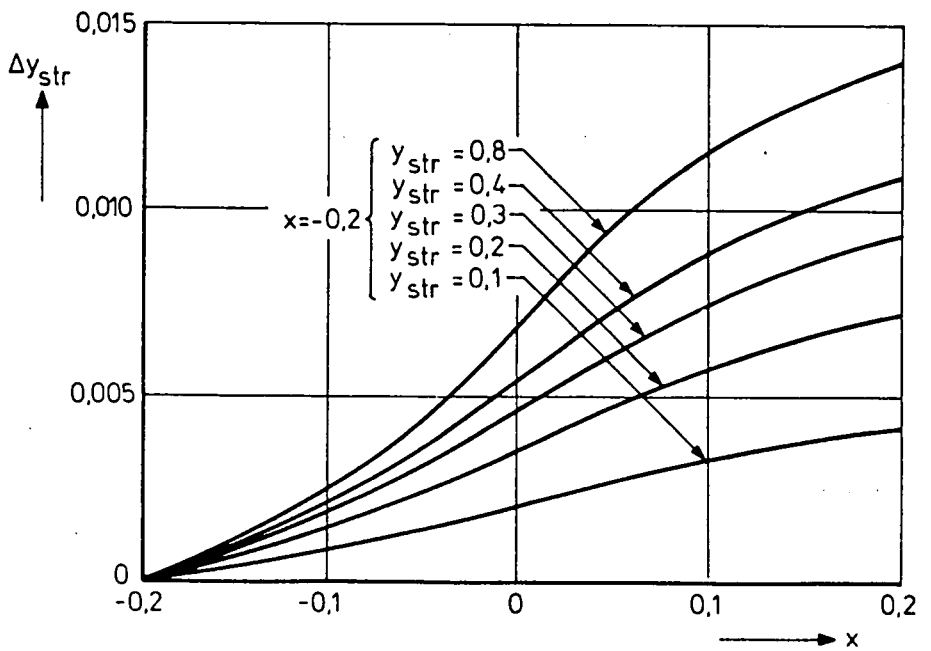

Fig. 25 : Streamlines ; test case : M = 1.12 , Re = $6.0 \cdot 10^6$.